Annals of Biomedical Engineering, Vol. 30, pp. 917–926, 2002
Printed in the USA. All rights reserved.

0090-6964/2002/30(7)/917/10/$15.00

Effect of a Flow-Streamlining Implant at the Distal Anastomosis of a Coronary Artery Bypass Graft

ANDREAS S. ANAYIOTOS,[1] PEDRO D. PEDROSO,[1] EVANGELOS C. ELEFTHERIOU,[2] RAMAKRISHNA VENUGOPALAN,[1] and WILLIAM L. HOLMAN[3]

[1]Department of Biomedical Engineering, [2]Department of Mechanical Engineering, and [3]Division of Cardiothoracic Surgery, University of Alabama at Birmingham, Birmingham, AL

(Received 24 July 2001; accepted 8 June 2002)

Abstract—Intimal thickening in the coronary artery bypass graft (CABG) distal anastomosis has been implicated as the major cause of restenosis and long-term graft failure. Several studies point to the interplay between nonuniform hemodynamics including disturbed flows and recirculation zones, wall shear stress, and long particle residence time as possible etiologies. The hemodynamic features of two anatomic models of saphenous-vein CABGs were studied and compared. One simulated an anastomosis with both diameter and compliance mismatch and a curvature at the connection, analogous to the geometry observed in a conventional cardiothoracic procedure. The other, simulated an anastomosis with a flow stabilizing anastomotic implant connector which improves current cardiothoracic procedures by eliminating the distal vein bulging and curvature. Physiologic flow conditions were imposed on both models and qualitative analysis of the flow was performed with dye injection and a digital camera. Quantitative analysis was performed with laser Doppler velocimetry. Results showed that the presence of the bulge at the veno-arterial junction, contributed to the formation of accentuated secondary structures (helices), which progress into the flow divider and significantly affect radial velocity components at the host vessel up to four diameters downstream of the junction. The model with the implant, achieved more hemodynamically efficient conditions on the host vessel with higher mean and maximum axial velocities and lower radial velocities than the conventional model. The presence of the sinus may also affect the magnitude and shape of the shear stress at locations where intimal thickening occurs. Thus, the presence of the implant creates a more streamlined environment with more primary and less secondary flow components which may then inhibit the development of intimal thickening, restenosis, and ultimate failure of the saphenous vein graft. © *2002 Biomedical Engineering Society.* [DOI: 10.1114/1.1500407]

Keywords—Coronary artery bypass graft, Hemodynamics, Flow visualization, Vascular flow modeling.

Address correspondence to Andreas Anayiotos, Associate Professor, Department of Biomedical Engineering, University of Alabama at Birmingham, Birmingham, AL 35294-4440. Electronic mail: aanayiot@eng.uab.edu

INTRODUCTION

A significant number of coronary artery bypass grafts fail postoperatively due to intimal hyperplasia (IH) and restenosis within months or years.[8,15,22] Studies on the mechanism underlying IH of grafts have shown a consistent correlation between its pathogenesis and hemodynamic factors and graft/artery compliance mismatch.[1–3,6,7,12,17,19,25,26] Hemodynamic factors such as low wall shear stress (WSS), high oscillatory shear stress in connection with a moving stagnation point, and large spatial gradients of wall shear stress have been implicated as causes of IH. Studies done by Ojha *et al.*[23] and Keynton *et al.*[16] using end-to-side anastomoses revealed low WSS predominantly distal to the toe on the wall opposite the floor, inside the proximal outflow segment (POS) and near a floor stagnation point. Loth *et al.*[21] studied steady flow velocity and WSS distribution in a polytetrafluoroethylene (PTFE) end-to-side anastomosis model representative of femoro-popliteal bypass in humans and ilio-femoral in canines. It incorporated typical realistic geometric parameters of anastomosis constructed by vascular surgeons. The model was scaled up in size, physiologic Reynolds number, and flow divisions were used including graft to artery diameter ratio and other important features. Their study characterized wall shear stress gradients (WSSG) at several locations with patent proximal outlet segment. WSSG was found low on the circumference of the hood, the floor, and sidewalls near the floor stagnation point. Flow separation was observed along the hood near the inside POS distal to the toe, inside POS proximal to heel, and sidewalls as flow enters anastomosis.

The anastomotic bed wall shear stress patterns are also influenced by the anastomotic geometry and the local blood flow wave form, as reported by Ethier *et al.*[13] The vascular geometry, surgical technique, and type of vascular prosthesis may influence graft–artery compliance mismatch. The vascular geometry can vary in many

ways such as ratio of graft–artery diameter, graft angle, and hood length.[21]

Since intimal thickenings occur at suture lines, *in vitro* graft models vary in terms of graft geometry, flow conditions, flow divisions, and graft angles. Ojha *et al.*[23] used a 45° graft model under steady and pulsatile flow conditions with proximal outflow segment occluded, which demonstrated the type of flow structures inside end-to-side vascular grafts with equal diameters and hood length ratio of 1.4. Lei[18] studied the effect of reducing the local WSSG by altering the junction geometry via computer aided design improvements and incorporating a Taylor model. Keynton *et al.*[16] studied the effect of graft angle on the local velocity field inside graft model under steady flow and POS occluded. Crawshaw *et al.*[9] studied flow disturbances at the distal end-to-side anastomosis and the effect of outlet flow conditions and Reynolds number on the floor phenomena using flow visualization. White *et al.*[26] studied flow behavior in models under steady and pulsatile conditions, different flow divisions, Reynolds number, and hood length to identify regions of low wall shear, oscillatory shear, and long partial residence time, to suggest a relation to localization of vascular intimal thickening. They observed the presence of a three-dimensional (3D) separation region, which originated from the heel and moved to the sinus region.

Several devices are presently utilized in the area of interventional cardiology including stents and grafts. Stents are minimally invasive wire mesh tubes, which act as scaffolds to keep narrowed or diseased vessels open. Vascular grafts, on the other hand, serve to replace or repair diseased vessels and can be from autologous parts of the body or synthetically made. Both stents and grafts have been used in coronary arteries as adjunct to angioplasty to keep the vessel from narrowing or as a patch material in end-to-side anastomosis to reduce suturing at the junction and to streamline the flow. The performance of such devices under hemodynamic conditions has not been extensively studied. Peacock *et al.*[24] investigated the effect of coronary artery stents on the flow characteristics. They and reported mild downstream flow instabilities, which may be important in the process of restenosis. Berry *et al.*[4] reported flow disturbances associated with the compliance mismatch in stented vascular segments. Berry *et al.*[5] reported that wire spacing in stented vascular segment models influenced dye washout times in flow visualization studies with dye injection.

Coronary Artery Anastomosis

The coronary artery in adults varies between 2 and 6 mm depending on gender, age, and condition. The size of the saphenous vein graft is usually larger than the coronary artery by sometimes as much as 30% in diameter.[11]

The coronary artery saphenous vein graft (SVG) procedure consists of harvesting the vein and making an incision in the shape of a crescent on the host vessel to attach the anastomosis by the surgeon's own judgment and standards. These criteria are not consistent and vary from patient to patient. In collaboration with the Department of Cardiothoracic Surgery we inspected several end-to-side SVG anastomotic procedures. Each procedure and anastomotic location varied significantly depending on the condition of the coronary vasculature, location of stenosis, and location of collateral vessels. In addition, the anastomotic angle between the host vessel and the anastomosis varied from approximately 20° to 70° and the anastomotic graft contained a curve close to the host vessel to facilitate and accommodate attachment. In addition, the anastomosis was not usually planar in geometry.

A unique feature of the saphenous vein anastomosis graft geometry is a bulge that forms at the veno-arterial junction when the saphenous vein section is exposed to the arterial pressure conditions of the coronary artery. This is usually first observed a few weeks after the operation. The resultant sinus and the surrounding geometry contribute to a complicated region of highly disturbed flow at the flow divider and may have a primary role in restenosis and the ultimate failure of the graft.

Coronary Artery Anastomosis with Implant

An anticipated improvement in the anastomotic process may be achieved by the implantation of a fitting, which serves as a scaffolding device in the anastomosis and incorporates the saphenous vein to the host coronary vessel without suturing. The fitting used in this study was designed and manufactured by Advanced Bypass Technologies, Inc., Pleasanton, CA, as the first attempt in the design of a hemodynamically efficient fitting (Fig. 1). It is made of Ni–Ti and has the shape of a cylindrical channel. The upstream cross section of the device is circular with an area of 19.6 mm^2 and its downstream section has a cross section of quasielliptical shape with a slightly pointed end as shown. The cross-sectional area is 35 mm^2. It eliminates the bulging of the saphenous vein at the junction and aims in streamlining the flow (Fig. 2). At the distal section, the implant has struts for structural stability at the host vessel, while at the proximal section it has some smaller prongs to connect to the saphenous vein. The company is currently performing biocorrosion/biocompatibility tests *in vitro* and in animals before obtaining FDA permission to begin clinical trials.

Purpose of Study

The purpose of our study was to evaluate the possible improvement in the flow characteristics of an anastomosis in the presence of a flow stabilizing implant. To do

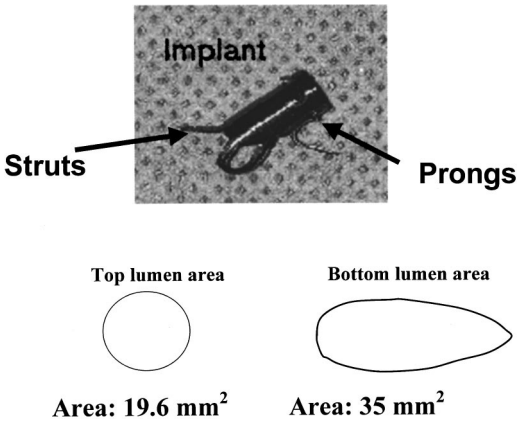

FIGURE 1. Anastomotic streamlining connector (Advanced Bypass Technologies).

so, the flow was evaluated in a conventional anatomic model of a coronary artery anastomosis, which exhibited some representative geometric features of the graft such as hood, curvature, and bulging at the junction.

This model was compared to an equivalent model of similar geometric features with a Ni–Ti graft implant designed to stabilize and streamline the flow by removing the curvature and bulging at the connection.

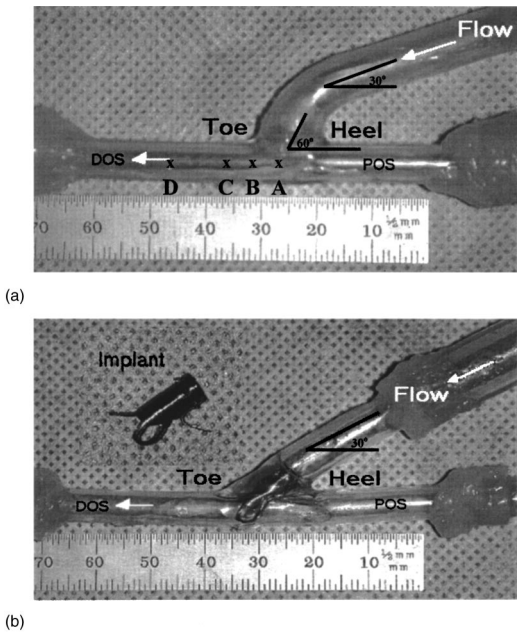

FIGURE 2. (a) Outline of the conventional anastomosis model with indication of measurement locations. A at the anastomotic flow divider, B one diameter downstream, C two diameters downstream, and D four diameters downstream. (b) Outline of the anastomosis with the implant.

METHODS

Model Construction

The two models were fabricated with the geometries shown in Figs. 2(a) and 2(b). The various parts and segments of each model are labeled, e.g., sinus, toe, heel, distal outflow segment (DOS), and proximal outflow segment.

Both models were designed in a planar fashion to simplify the construction procedure and the fluid dynamics. The anastomosis was at an angle of 30° with the host vessel for both models, since the design of the implant required a 30° anastomotic angle. We designed the vessel diameter to be 4.75 mm to maximize laser Doppler velocity (LDV) resolution even though the averaged coronary diameter is smaller. The anastomotic side was designed at 6.75 mm in diameter to simulate extreme diameter mismatch with the anticipated bulging of the graft. This combined effect accounted for the anastomotic diameter to be about 40% larger than the host diameter. In addition, the anastomotic side was designed with a curvature towards the host vessel, which started at 30° and connected with the host at an angle of 60°, as shown in Fig. 2(a).

The implanted model was designed with the same diameters of 4.75 and 6.75 mm for the host and graft, respectively. The implant in the simulated model was deployed and fastened using the same procedure as the one used during bypass surgery.

Therefore, the conventional model simulates a model of an anastomosis, representative of the cardiothoracic procedure, where the curvature at the hood is present where the anastomosis meets the host vessel, and the bulging is present following the exposure of the vein to the arterial pressure conditions. The implanted model simulates a more streamlined connection without a curvature or a bulge to elucidate the hemodynamic benefits of such a connection as designed by the manufacturer.

Solids and rapid prototype models of the interior volume of these vessels were created using I-DEAS solids modeling software and stereolithography. The rapid prototypes were polished and electroplated to prevent adhesion during the molding process. The models were then constructed of a silicone elastomer Sylard 184 (Dow Corning Midland, MI), which satisfied the requirements of a clear optical path. The flow area at the intersection of the conventional anastomosis model had an oval shape of an area of 33 mm^2 and the implant flow area had a quasielliptical shape with a total flow area of 35 mm^2, as shown in Fig. 1. The diameter of the coronary artery section was 4.75 mm and the saphenous section 6.75 mm. The thickness of both models varied between 0.9 and 1.1 mm and the thickness to diameter ratio was 0.24 for the host and 0.13 for the bypass and were within physiologic values.[10] The compliance of the model was

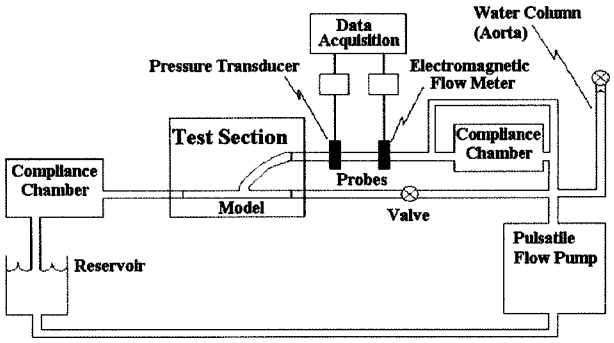

FIGURE 3. Flow system.

approximately 0.07% per mm of mercury for all sections of the model. This compares favorably with the coronary artery compliance of 0.59%, but less favorably with the saphenous vein compliance of 0.44%.[10]

Flow System

A schematic diagram of the flow setup is shown in Fig. 3. The blood mimicking fluid used was an aqueous solution of glycerin (36% glycerin by weight), which had a dynamic viscosity of 3.0 cP and density of 1086 kg/m^3. The anastomosis model was placed in a test fluid-filled tank to eliminate gravity-driven distortion and facilitate flow visualization. The proximal side of the graft was connected to an in-house constructed pulse duplication device. Compliance chambers, which served to control wave reflections and create a physiologic signal, were placed proximal to the graft inlet and distal to the exit of the host artery. The pump operated at 75 beats/min (1.25 Hz) and the total flow rate was 75 ml/min. Flow was monitored upstream and downstream of the test section by electromagnetic flowmeter probes to continuously monitor flow through the test section (FM 501, Carolina Medical Electronics, King, NC). Pressure was monitored upstream and downstream of the test section using Linear Variable Differential Transformer (LVDT) pressure transducers (Validyne, model DP15TL Northridge, CA). The transducers were calibrated in cm of water with a static water column. The upstream pressure wave form was taken from a subject who had received a saphenous vein graft and underwent diagnostic catheterization [Fig. 4(a)]. A comparison of the experimental and physiologic pressure wave forms are shown in Fig. 4(a) and the resulting flow wave form in Fig. 4(b).

A flow division of 100:0 distal to proximal outlet segment (DOS:POS) was maintained in the setup to simulate conditions of 100% stenosis in the proximal part of the host vessel with no flow upstream to possible collaterals. This simulated the extreme case.

All hemodynamic parameters (Reynolds number, flow rate, pressure) were within physiologic range. The peak

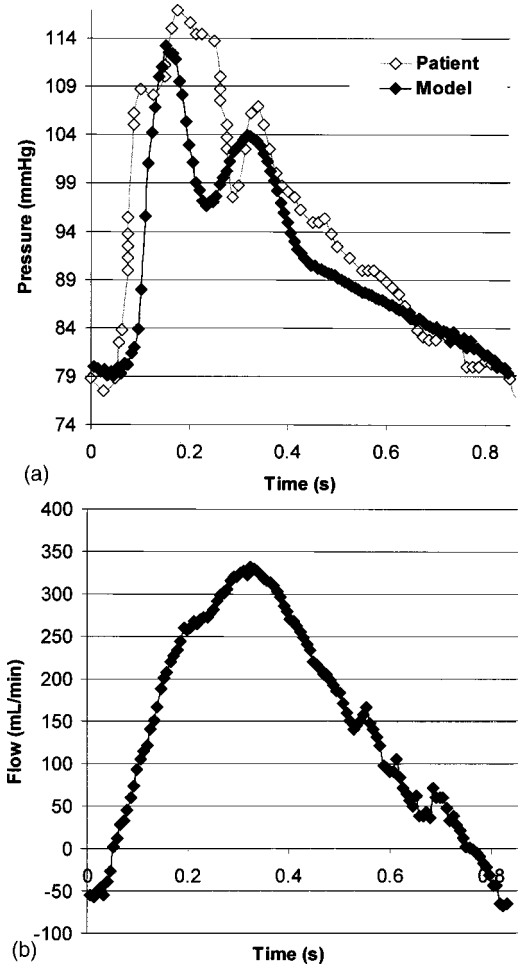

FIGURE 4. (a) Pressure wave form comparison between physiologic and experimental. (b) Flow wave form.

Reynolds number was 580 and the mean Reynolds was 200 based on the diameter of the coronary artery section (4.75 mm). The flow was 1 ml/stroke. The Womersley number was 1.5. Under these flow conditions, the conventional anastomosis model exhibited a diameter extension of about 3% at the coronary artery section and about 3.5% at the sinus section of the anastomosis. A 3% wall motion was also observed at the coronary and anastomotic sections of the implanted model.

Flow Visualization Setup

Food dye was dissolved in the mixture injected through a 20 gage needle through the proximal outflow section. The qualitative flow events were recorded on a digital camera, Nikon Coolpix 990, Nikon, Japan, with a resolution of 3.34 Mpixels, from lateral and top views. The camera was synchronized with the pulse duplication device to match flow images with cycle phase.

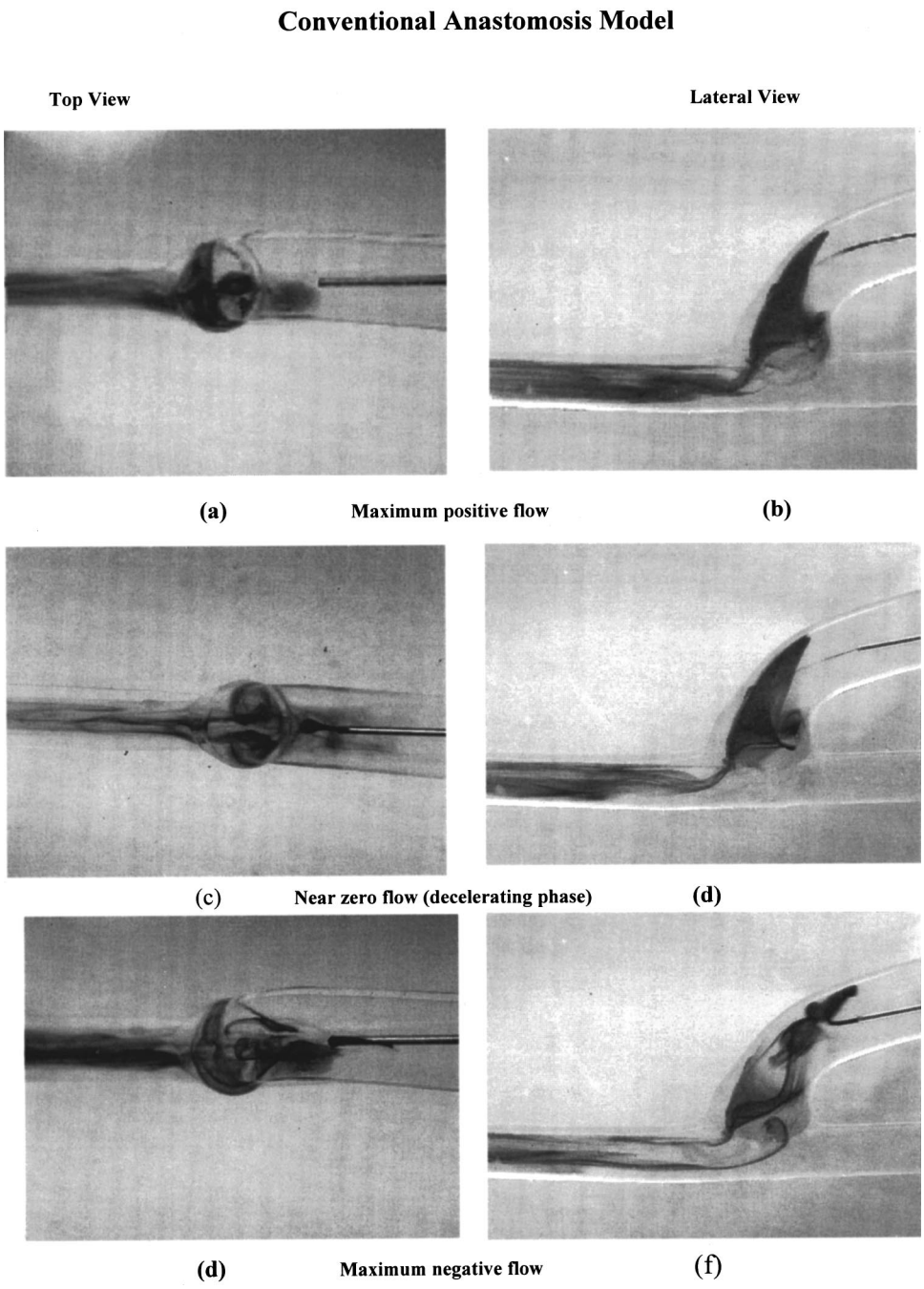

FIGURE 5. (a)–(f) Qualitative flow features visualized in the conventional anastomosis model (top and lateral views).

Laser Doppler Velocimetry Setup

Dantec Electronics (Mahwah, NJ) provided the one-dimensional LDV system. This system utilized a Uniphase 20 mW He–Ne laser tube as the coherent light source. The LDV sample volume dimensions were 1.5 $\times 0.2 \times 0.2$ mm. A computer-controlled traverse table provided the means for positioning the laser optical transducer. The axial and radial velocity components were measured at each site. FLOWARE, a software package used in the operation of the Dantec LDV system, acquired and processed the velocity data. Average sampling rates ranged from 100 to 200 Hz and remained relatively constant throughout the data acquisition. Four critical points were selected as the measurement locations within the coronary vessel. Point A at the center of the connection, point B right below the toe, point C two diameters from the center of the connection, and point D four diameters from the center of the connection. The

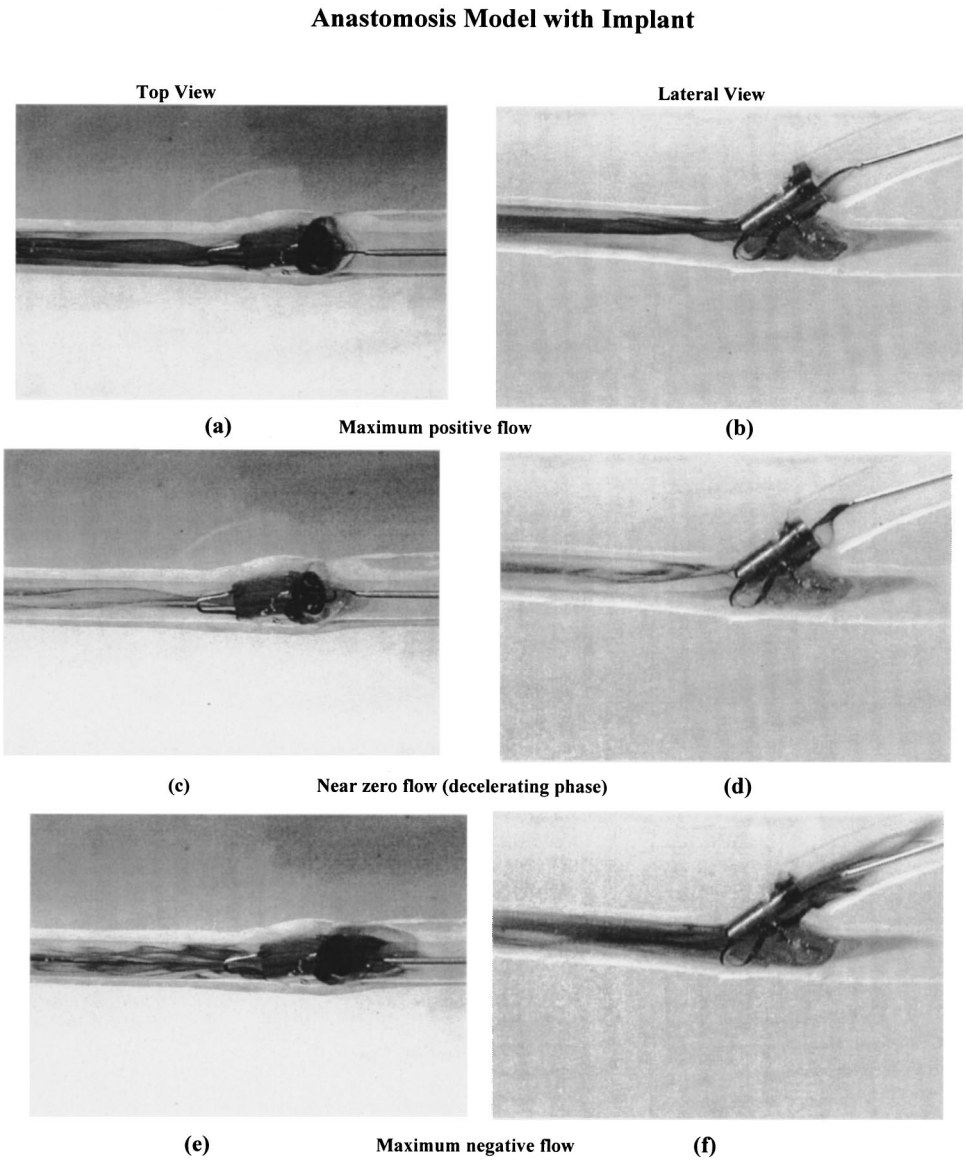

FIGURE 6. (a)–(f) Qualitative flow features visualized in the implanted anastomosis model (top and lateral views).

interrogation process utilized the small dimensions of the laser sample volume, thus accessing the centerline of each measurement point from the top wall to the bottom wall. The sample volume was first focused on the top wall, which served as the reference point in locating each of the measurement points. The calculation of the exact location of the sample volume considered the beam angle and optical refraction.

RESULTS

Flow Visualization

The dye trajectories indicated a region of highly disturbed flow at the connection. At the bulge, exchanges in momentum from axial to radial and vice versa throughout the cardiac cycle were evidenced by significant secondary structures throughout the cycle. This included two antisymetric helices covering the whole cross section with strongest radial velocity components at end diastole. Flow separation seemed predominant at the heel as well as the toe. The secondary flow structures propagated into the main branch and showed shedding into the proximal part of the coronary artery branch (POS) on the side of the stenosis, indicating regions of flow stasis and low and oscillating shear stress. Their significance downstream of the flow divider could not be qualitatively assessed due to the small scale of the model. A stagnation point was qualitatively located directly below the flow divider. The qualitative flow features are shown in Figs. 5(a)–5(f).

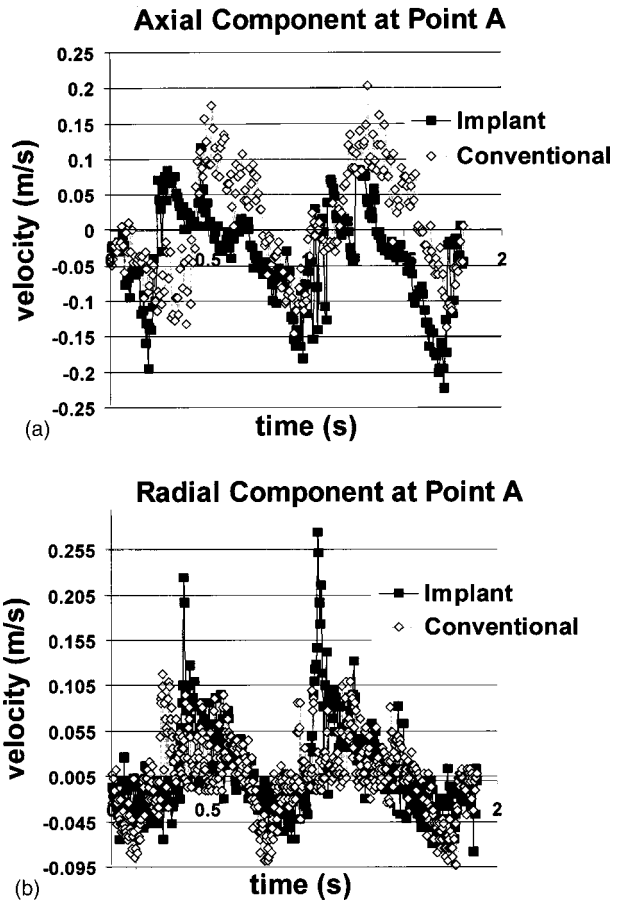

FIGURE 7. (a) Axial velocity component at A [at the anastomotic flow divider as shown in Fig. 2(a)] for each model. (b) Radial velocity component at A for each model.

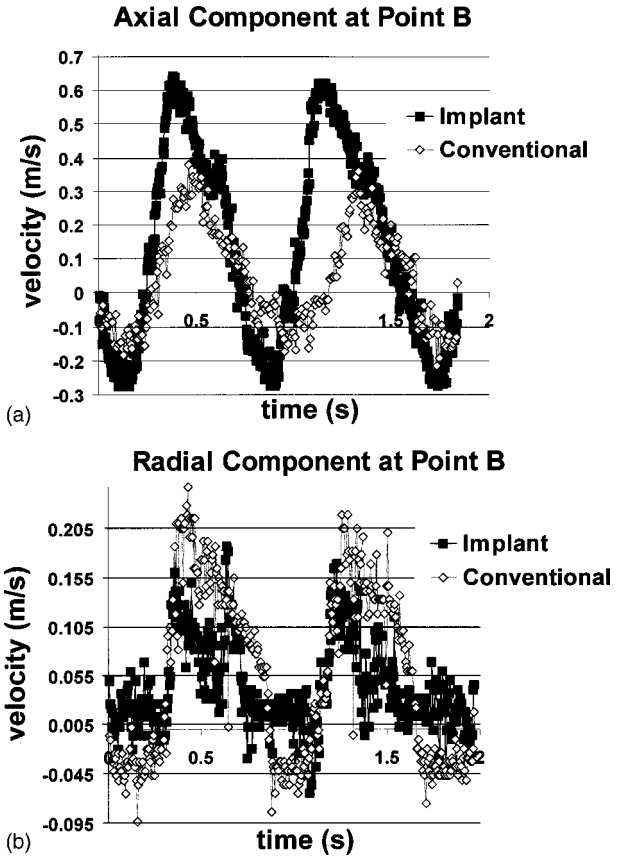

FIGURE 8. (a) Axial velocity component at B (one diameter from the anastomotic flow divider) for each model. (b) Radial velocity component at B for each model.

Anastomosis Model with the Implant

For the model with the implant, the general features of anastomotic flow such as flow separation and disturbed multidirectional flow, were still present; however, the features appear more streamlined than those in the conventional model [Figs. 6(a)–6(f)]. A disturbance upstream of the connection at the rigid compliant interface was observed, which may be a result of the geometric discontinuity and compliance mismatch Figs. 6(b) and 6(c).

Laser Doppler Velocimetry

The quantitative flow features in the form of velocity time histories at points A, B, C, and D [Fig. 2(a)] between the conventional anastomosis model (CAM) and the implanted anastomosis model (IAM) are compared below.

Point A. This is a location right at the center of the flow divider. Axial velocities varied between -0.14 and 0.2 m/s in the CAM and between -0.2 and 0.12 m/s for the IAM [Fig. 7(a)]. The two wave forms were disturbed and showed sudden temporal and spatial velocity gradients and reversal of direction. The radial velocities also indicated a high level of local disturbances. The magnitudes varied from -0.09 m/s to 0.11 s for the CAM and -0.06 to 0.25 m/s for the IAM [Fig. 7(b)].

Point B. Right below the toe, it is seen that the IAM exhibited significantly higher axial velocity magnitude and variations than the CAM [Fig. 8(a)]. The character of the IAM wave form also showed fewer local disturbances than the CAM. The IAM wave form varied between -0.27 and 0.65 m/s and the CAM wave form between -0.18 and 0.39 m/s. The increase in momentum in the axial direction in the IAM case coincided with a lowering effect on the radial velocity magnitude and its variation, as shown in Fig. 8(b). Radial velocity variation for the IAM was between -0.07 and 0.18 m/s, while for the CAM it was higher, and varied between -0.10 and 0.25 m/s.

Point C. Two diameters from the center of the connector, the IAM showed an even higher tendency towards

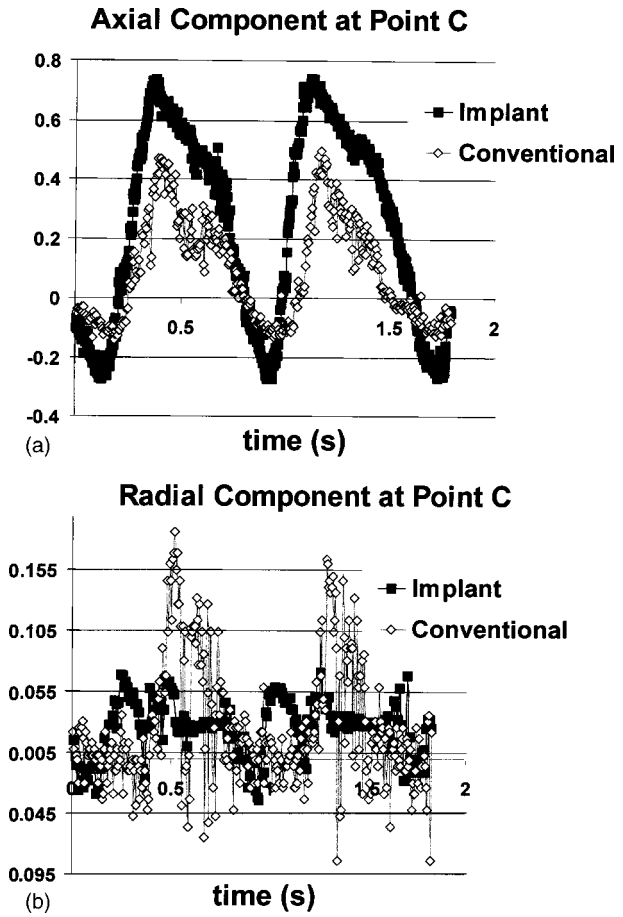

FIGURE 9. (a) Axial velocity component at C (two diameters from the anastomotic flow divider) for each model. (b) Radial velocity component at C for each model.

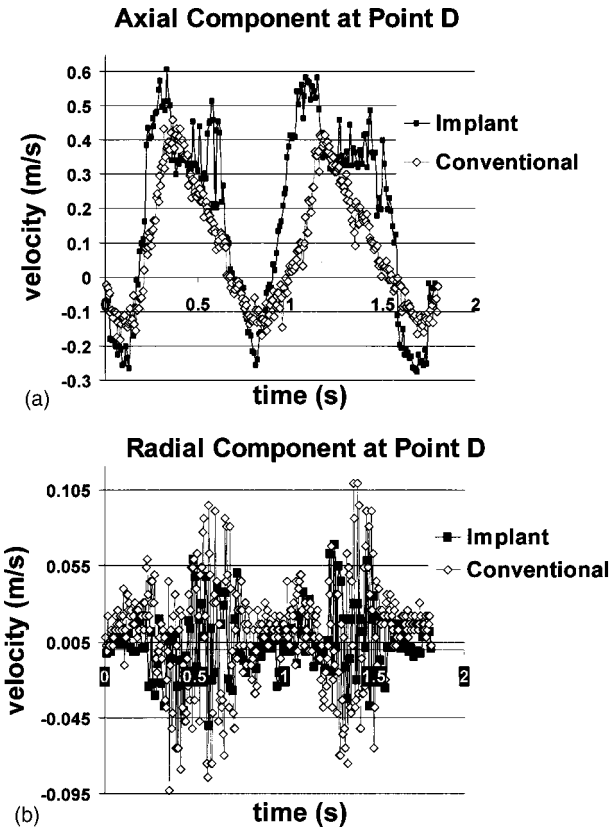

FIGURE 10. (a) Axial velocity component at D (four diameters from the anastomotic flow divider) for each model. (b) Radial velocity component at D for each model.

alignment in the axial direction with an axial velocity magnitude variation from −0.26 to 0.71 m/s in contrast to −0.13 and 0.46 m/s for the CAM [Fig. 9(a)]. In the radial direction, the velocity component of the IAM was reduced to the range of −0.03 to 0.07 m/s. The CAM maintained a much higher radial velocity magnitude and ranged between −0.09 and 0.011 m/s [Fig. 9(b)].

Point D. Finally, four diameters from the center of the flow divider, the axial velocity wave forms show similar features between the two models [Fig. 10(a)]. The magnitudes varied between −0.027 and 0.6 m/s for the IAM and −0.19 and 0.46 m/s for the CAM. In the radial direction the CAM preserves the radial component of the velocity more than the IAM, as shown in Fig. 10(b). The IAM radial velocity varies from −0.05 to 0.06 m/s while the CAM oscillates between −0.1 and 0.1 m/s [Fig. 10(b)].

The maximum, minimum, and mean values of velocities at each point and direction are shown in Figs. 11(a)–11(f).

DISCUSSION

This study compared the qualitative and quantitative differences of the general flow characteristics of two models which simulated a conventional anastomosis (CAM) and one with an implant (IAM). The anastomotic model without the implant showed that three-dimensional helical patterns were present in the anastomotic junction and were accentuated in the presence of the sinus and point of curvature. Regions of disturbed, separated, stagnant, and oscillatory flow were identified from the flow visualization and LDV experiments and confirm earlier studies with scaled up models.[20,21,25]

The flow visualization data indicated a flow disturbance observed at the upstream interface between the rigid implant and the compliant wall of the anastomosis [Figs. 6(b) and 6(c)] can be explained by geometric considerations. The thickness of the implant is about 0.5 mm and the diameter is 5 mm. This rigid end connects to a compliant 7 mm diam vessel, which creates a diameter mismatch and also a compliance mismatch. Redesigning the implant to avoid this mismatch would be necessary in an improved design prior to clinical implementation.

The purpose of the implant was first to minimize suturing and trauma and then to streamline the flow.

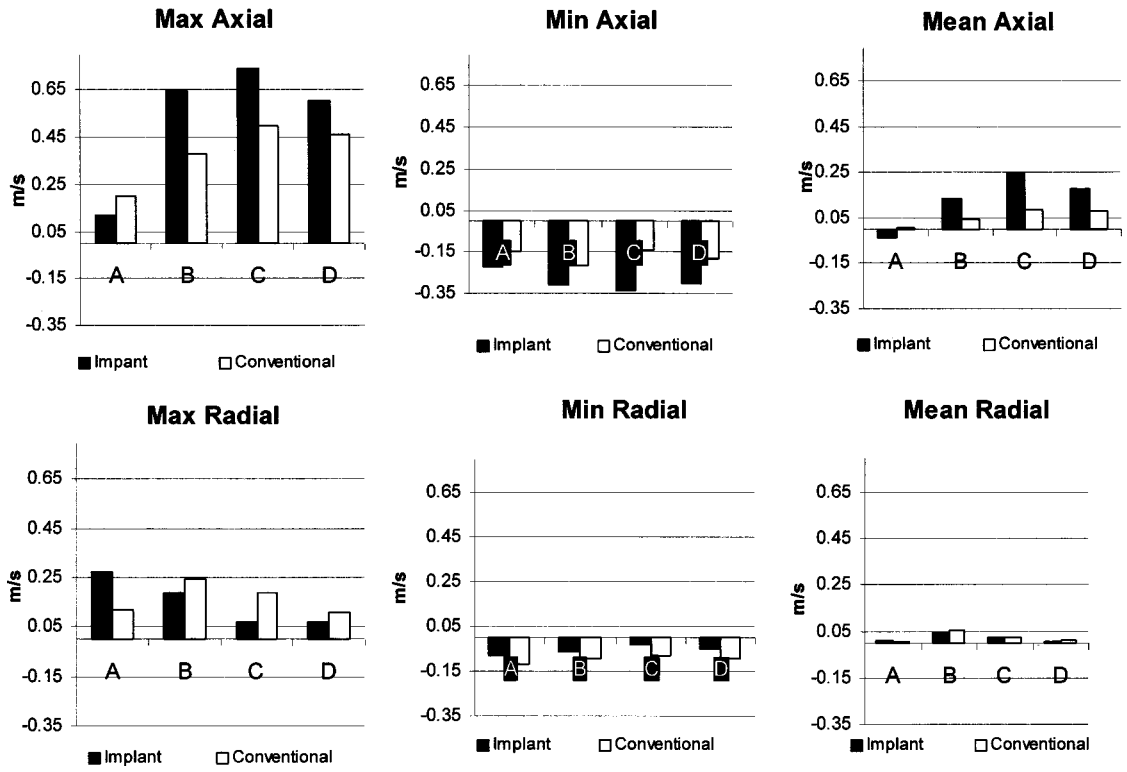

FIGURE 11. Statistical comparison of maximum, minimum, and mean axial and radial velocity for each measurement location.

Inevitably, the implant cannot avoid the inherent characteristics of anastomotic flow such as separation at the toe and heel, formation of a stagnation point at the bed of the host vessel, and vortex shedding into the proximal outflow track (POS). However, the cylindrical, rigid NiTi implant did provide streamlining of the flow at the junction, and reduced the disturbances at the sinus and downstream, as evidence by the laser Doppler velocity data along the centerline of each model. The effect is most profound at locations B and C where the axial components at the centerline were much greater in the IAM than the CAM with fewer local disturbances. The increase in the axial component was accompanied by a decrease of the radial component. Hence, at the same locations B and C, the IAM radial velocity components were lower than the corresponding of CAM (Figs. 8 and 9). This shows that the presence of the streamliner preserves the momentum in the axial direction and reduces the conversion of momentum to secondary directions. In the CAM the helices created due to the curvature and sinus geometry at the connection influenced the downstream features of the flow in the host vessel, causing the momentum to be reduced in the axial direction and increased in the radial direction. The increased radial velocity magnitude is preserved in the CAM even four diameters from the connection at point D [Fig. 10(b)]. Comparison of the maximum, minimum, and mean values of the velocity at each point shows that for points B, C, and D, the maximum, minimum, and mean axial velocities are higher in the IAM while the maximum, minimum, and mean radial velocities are higher in the CAM, thus confirming the presence of higher axial momentum in the host vessel section of the IAM.

Further near-wall quantitative information with LDV and with CFD studies are necessary to provide precise information on the details of the near-wall flow phenomena and to further assess the hemodynamic performance of the implant. Such information will be available in the near future and will be vital in the future improvement of the implant design.

In conclusion, the qualitative and quantitative studies performed showed streamlining of the flow at the junction and the reduction of secondary structures in the model with the implant. This alone is a positive factor since the axial component of the velocities has been increased at the expense of the radial components, therefore, more energy is used to drive blood flow forward and less energy is wasted in creating secondary flow structures and recirculation, which contribute to flow stasis. The reduction of disturbances alone may be a favorable factor against the formation of intimal hyperplasia.

Limitations

Our study used only one flow division ratio, namely, no flow through the proximal outflow section. This represents the hemodynamically worst-case situation of a completely occluded coronary vessel and no flow to collateral vessels. Different flow division ratios through the POS could provide more information regarding the function and efficiency of the model. Guo *et al.*,[14] however support the idea that anastomoses should be connected close to the stenosis to avoid a flowfield to the collaterals, which deteriorates the hemodynamic conditions at the anastomotic junction.

In addition, even though the models were compliant and exhibited realistic wall motion, their compliance characteristics are different than the physiologic compliance of a coronary artery bypass graft, which may affect the compliance mismatch characteristics (see, also, Refs. 1, 2, 6, 7, 12, 14, 15, and 17).

ACKNOWLEDGMENT

The authors wish to express their thanks to Advanced Bypass Technologies for their financial support of the project.

REFERENCES

[1] Anayiotos, A. S., D. P. Giddens, S. A. Jones, S. Glagov, and C. K. Zarins. Shear stress at a compliant model of the human carotid bifurcation. *J. Biomech. Eng.* 116:98–106, 1994.

[2] Asakura, T., and T. Karino. Flow patterns and spatial distribution of atherosclerotic lesions in human coronary arteries. *Circ. Res.* 66:1045–1066, 1990.

[3] Bassiouny, H. S., S. White, S. Glagov, E. Choi, D. P. Giddens, and C. K. Zarins. Anastomotic intimal hyperplasia: mechanical injury or flow induced. *J. Vasc. Surg.* 15:708–717, 1992.

[4] Berry, J. L., J. E. Moore, V. S. Newman, and W. D. Routh. *In vitro* flow visualization in stented arterial segments. *J. Vasc. Invest.* 3:63–68, 1997.

[5] Berry, J. L., A. Santamaria, J. E. Moore, V. S. Newman, S. Roychowdhury, and W. D. Routh. *In vitro* flow visualization in stented arterial segments. *Ann. Biomed. Eng.* 28:386–398, 2000.

[6] Braunwald, Heart Disease: A Textbook of Cardiovascular Medicine, 5th ed., 1997, pp. 1317–1326.

[7] Butany, J. W., T. E. David, and M. Ojha. Histological and morphometric analyses of early and late aortocoronary vein grafts and distal anastomoses. *Can. J. Cardiol.* 14:671–677, 1998.

[8] Canver, C. C. Conduit options in coronary artery bypass surgery. *Chest* 108:1150-1155, 1995.

[9] Crawshaw, H., and W. Quist. Flow disturbance at the distal end-to-side anastomosis. *Arch. Surg. (Chicago)* 115:1280–1284, 1980.

[10] David, G., and C. Andreas. Review of Physiology, Appleton and Langes', 1997.

[11] Davies, P. F. Flow mediated endothelial mechanotransduction. *Physiol. Rev.* 75:519–560, 1995.

[12] Echave, V., and A. Koornick. Intimal hyperplasia as a complication of the use of PTFE graft for femoral popliteal. *Bypass Surg.* 86:791–798, 1979.

[13] Ethier, C. R., D. A. Steinman, X. Zhang, S. R. Karpik, and M. Ojha. Flow wave-form effects on end-to-side anastomotic flow patterns. *J. Biomech.* 31:609–617, 1998.

[14] Guo, L., D. A. Steinman, B. C. Moon, W. Wan, and R. J. Milsap. Effect of distal graft anastomosis site on retrograde perfusion and flow patterns of native coronary vasculature. *Ann. Thorac. Surg.* 72:782–787, 2001.

[15] Imparato, A., and A. Bracco. Intimal and neointimal fibrous proliferation causing failure of arterial reconstructions. *Surgery (St. Louis)* 72:1007–1017, 1972.

[16] Keynton, R. S., S. E. Rittgers, and M. C. S. Shu. The effect of angle and flow upon hemodynamics in distal vascular graft anastomoses: An *in vitro* model study. *J. Biomech. Eng.* 113:458–463, 1991.

[17] Ku, D., D. P. Giddens, C. K. Zarins, and S. Glagov. Pulsatile flow and atherosclerosis in the human carotid bifurcation: Positive correlation between plaque location and oscillating shear stress. *Arteriosclerosis (Dallas)* 5:293–302, 1985.

[18] Lei, M., C. Kleinstreuer, and J. P. Archie. Hemodynamic simulations and computer-aided designs of graft–artery junctions. *J. Biomech. Eng.* 119:343–348, 1997.

[19] Logerfo, F., and W. Quist. Downstream anastomotic hyperplasia: A mechanism of failure in Dacron arterial grafts. *Ann. Surg.* 197:479–483, 1987.

[20] Louagie, Y., and J. P. Haxhe. Intraoperative electromagnetic flowmeter measurements in coronary artery bypass grafts. *Ann. Thorac. Surg.* 57:35–64, 1994.

[21] Loth, F., S. A. Jones, D. P. Giddens, H. S. Bassiouny, S. Glagov, and C. K. Zarins. Measurements of velocity and wall shear stress inside a PTFE vascular graft model under steady flow conditions. *J. Biomech. Eng.* 119:187–94, 1997.

[22] Lytle, B. W., F. D. Loop, and D. S. Cosgrove. Long term serial studies of internal mammary artery and saphenous vein coronary bypass grafts. *J. Thorac. Cardiovasc. Surg.* 89:248–258, 1995.

[23] Ojha, M., C. R. Ethier, K. W. Johnston, and R. S. C. Cobbold. Steady and pulsatile flow in an end-to-side arterial anastomosis model. *J. Vasc. Surg.* 12:747–753, 1990.

[24] Peacock, J., S. Hankins, T. Jones, and R. Lutz. Flow instabilities induced by coronary artery stents: Assessment with an *in vitro* pulse duplicator. *J. Biomech.* 28:17–26, 1995.

[25] Sottiurai, V. S., J. S. T. Yao, R. C. Batson, S. L. Sue, R. Jones, and Y. A. Nakamura. Distal anastomotic hyperplasia: Histopathologic character and biogenesis. *Ann. Vasc. Surg.* 3:26–33, 1989.

[26] White, S. S., C. K. Zarins, D. P. Giddens, H. Bassiouny, F. Loth, S. A. Jones, and S. Glagov. Hemodynamic patterns in two models of end-to-side vascular graft anastomoses: Effects of pulsatility, flow division, Reynolds number, and hood length. *J. Biomech. Eng.* 115:104–111, 1993.